This is the accepted version of the following article:

Fariña Santana D., Álvarez M., Márquez S., Domínguez C., Lechuga L.M.. Out-of-plane single-mode photonic microcantilevers for integrated nanomechanical sensing platform. Sensors and Actuators, B: Chemical, (2016). 232. : 60 - . 10.1016/j.snb.2016.03.041,

which has been published in final form at https://dx.doi.org/10.1016/j.snb.2016.03.041 © https://dx.doi.org/10.1016/j.snb.2016.03.041. This manuscript version is made available under the CC-BY-NC-ND 4.0 license http://creativecommons.org/licenses/by-nc-nd/4.0/

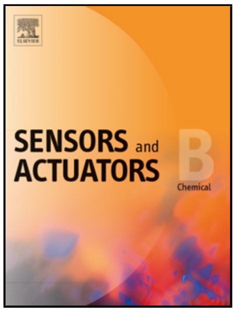

Title: Out-of-plane single-mode photonic microcantilevers for integrated nanomechanical sensing platform

Author: D. Fariña M. Álvarez S. Márquez C. Domínguez L.M. Lechuga

PII: S0925-4005(16)30335-5
DOI: http://dx.doi.org/doi:10.1016/j.snb.2016.03.041
Reference: SNB 19846

To appear in: *Sensors and Actuators B*

Received date: 17-11-2015
Revised date: 9-3-2016
Accepted date: 10-3-2016

Please cite this article as: D.Fariña, M.Álvarez, S.Márquez, C.Domínguez, L.M.Lechuga, Out-of-plane single-mode photonic microcantilevers for integrated nanomechanical sensing platform, Sensors and Actuators B: Chemical http://dx.doi.org/10.1016/j.snb.2016.03.041

This is a PDF file of an unedited manuscript that has been accepted for publication. As a service to our customers we are providing this early version of the manuscript. The manuscript will undergo copyediting, typesetting, and review of the resulting proof before it is published in its final form. Please note that during the production process errors may be discovered which could affect the content, and all legal disclaimers that apply to the journal pertain.

Out-of-plane single-mode photonic microcantilevers for integrated nanomechanical sensing platform

D. Fariña [ab], M. Álvarez [ba], S. Márquez [ba], C. Domínguez [c], L. M. Lechuga[ba*]

a. CIBER-BBN Networking Center on Bioengineering, Biomaterials and Nanomedicine, Spain.
b. Nanobiosensors and Bioanalytical Applications Group, Catalan Institute of Nanoscience and Nanotechnology (ICN2), CSIC and The Barcelona Institute of Science and Technology, Campus UAB, Bellaterra, 08193 Barcelona, Spain
c. Microelectronics Institute of Barcelona (IMB-CNM), CSIC, Barcelona, Spain.

Corresponding author: Laura M. Lechuga, email: laura.lechuga@cin2.es

Highlights

- A high sensitive out-of-plane single-mode optical microcantilever, is used to detect the human grow hormone.
- The out-of-plane single-mode optical device is fabricated with the optimized dimensions.
- An optical custom setup, with auto-alignment system, allows to increase the signal to noise ratio.
- The optical device bending is demonstrated with a polyelectrolyte bilayers conformation.

Keywords: BioMEMS, cantilever, optical, human growth hormone.

Abstract

We have studied the optomechanical performance of optical microcantilevers fabricated with integrated waveguides for the on-chip and real-time detection of biorecognition events. The nanomechanical photonic device consists of an optical microcantilever with on-chip integrated waveguides for both coupling the light and detecting the microcantilever response. The photonic device was designed to reach a high sensitivity with a low deflection noise density (DND) of only $0.13\, fm/\sqrt{Hz}$. The BioMEMS transducer is embedded into a proper designed PMMA/PDMS microfluidic header and connected to a flow delivery system to study the response of the fully-integrated device under physiological conditions. As a proof of concept, we have studied the photonic microcantilever bending during consecutive formation of ultrathin polyelectrolyte multilayer films (electrostatic binding) and during biofunctionalization and biorecognition of the human growth hormone. The read-out platform was developed based on a single laser–single acquisition channel. To avoid the effect of external factors such as device positioning or temperature fluctuations, an automatized light coupling system keeps on tracking the laser beam focused into an input waveguide, increasing the required reproducibility needed for BioMEMS devices and paving the way for a potential portable multichannel sensor platform.

1 Introduction

One of the key advantages of lab-on-chip (LOC) biosensor technology is that they can achieve comparable sensitivity and specificity, or even higher, to those obtained with the well-established techniques used in centralized laboratories or diagnostic services [1–3]. The final aim of any LOC biosensor technology is to provide a fully integrated, cheap, portable and reliable platform, able to detect and identify simultaneously different analytes in real time with relevant sensitivity; always looking for an easy-to-use and disposable diagnostic tests directly run by the consumer. Currently, most commercialized LOCs are easy to handle devices for the detection of a specific compound based on simple sensors, mainly with a binary output response (positive/negative). However, obtaining a quantitative result requires more complex sensors and instrumentation for the reading and interpretation of the signals. Most of these approaches employ labelling or amplification techniques, such as fluorescent, chemo-luminescent, redox-active, enzyme, or nanoparticles [4–6], which are laborious, time and sample consuming and limited the number of analytes that can be studied, which is quite far from the traditional vision of a LOC device.

A promising method to accomplish a cost-effective real integrated LOC/biosensor device is based on Micro and Nano-electro-mechanical system (MEMS, NEMS). Biosensors based on MEMS offer many of the properties required for that goal, such as a tiny sensor area, a label-free detection method, low-cost fabrication and mass production, and compatibility with CMOS (complementary metal-oxide semiconductor) technology that can be easily scaled up. Currently it is possible to fabricate arrays of tens to thousands of microcantilevers. MEMs based biosensors have already demonstrated a very high sensitivity for molecular diagnostic or even for single cell detection [7–9]. However the multiplexed capability for monitoring several compounds still present some limitations related with the read-out methodology (critical alignment, initial bending or integration). To solve these limitations a new method based on the integration of in-plane photonic transduction for microcantilevers was first introduced by our Group [10]. This approach led to the successful fabrication of highly integrated sensors based on silicon or polymer technology by other groups [10–12], demonstrating the application of a single microcantilever as chemical sensor [12,13]. Recently, Nordin et al. have demonstrated the transient response of an array of photonic microcantilevers with integrated PDMS-based microfluidic for biosensing of streptavidin [14].

In this work, we present a full system based on an array of optical waveguide microcantilevers (OWC) and demonstrate the optomechanical performance of these transducers as biosensors. Two key features of any biosensor device are its sensitivity and reproducibility, which are mainly defined by the transducer and by the biofunctiolization process. Therefore, we have employed an automatic experimental set-up, which maximizes the light coupling into each microcantilever, increasing the reproducibility and preventing drifts of the collected signal due to losses in the light in coupling. We demonstrate the suitability of our sensor system by evaluating in real time the formation of ultrathin polyelectrolytes multilayers in liquid environment. As a proof of concept as a biosensor, we also demonstrate the suitability of the sensor system as an immunosensor for label-free detection of the human growth hormone (hGH) by its corresponding monoclonal antibody, previously immobilized on the cantilever surface.

2 Optical Waveguide Cantilevers

2.1 OWC device working principle

Figure 1 shows the design and the working principle of the nanomechanical photonic transducer. The device is a SiO_2 microcantilever, acting as an out-of-plane single-mode optical waveguide, aligned with an out-of-plane input and output Si_3N_4 waveguide (Figure 1-A). The Si_3N_4 waveguides are covered by a SiO_2 cladding layer, getting a symmetric out-of-plane single-mode waveguide. The light propagating through the input waveguide is coupled into the microcantilever mainly by the evanescent field of the electromagnetic wave, with a coupling efficiency of 50% [15]. The nanomechanical response of the microcantilever operating in static mode, is due to a surface stress, $\Delta\sigma$, motivated by a molecular interaction (Figure 1-B), that is monitored by the changes in the optical power coupled into the output waveguide.

Light exiting the microcantilever free-end is propagated across the gap and coupled into the out-of-plane single-mode output waveguide. When the position of the microcantilever free-end changes, the light coupled into the output waveguide also changes following a Gaussian response related with a single-mode profile (Figure 1-C). The initial misalignment between the microcantilever and the output waveguide makes possible to distinguish between the up and down deflection of the microcantilever, increasing the collected power for the upside bending and decreasing for the downside one, respect to the initial flat position. Finite Elements Method were computed to maximize the device sensitivity up to $S = 4.8\text{x}10^{-2}\ \text{nm}^{-1}$ (Figure 1-D) and to achieve maximal output efficiency of η = 19.9 % at zero OWC deflection, for an OWC thickness of 350 nm with 1 µm gap distance and input and output Si_3N_4 waveguides thickness of 130 nm [15].

2.2 Fabrication of the OWC devices

The dimensions of the photonic microcantilever device were chosen to achieve an out-of-plane single-mode behavior and to improve simultaneously the mechanical and the optical performance [15]. The devices were fabricated in a 10x8 mm chip, with a window in the middle of the chip, where an array of 18 SiO_2 microcantilevers is suspended (Figure 2-A). The microcantilevers are 100 µm long, 30 µm wide and 350 nm thick, with a refractive index of $n_{SiO_2} = 1.46$ (Figure 2-D). The input and output Si_3N_4 waveguides are 30 µm wide and 130 nm thick, with a refractive index of $n_{Si_3N_4} = 2.00$. The distance between the input waveguides end and the microcantilever clamping region is of 500 nm to avoid generation of stress on the microcantilever clamping region and to increase the power of light coupled through the evanescent field into de SiO_2 layer. The gap between the microcantilever free end and the output waveguide is 1 µm.

The fabrication process is summarized in Figure 2-E, starting with the growth of 2 µm of thermal SiO_2 on a 300 µm silicon wafer, which is the OWC structural material and also acts as cladding for the input and output waveguides. After that, a Si_3N_4 Low Pressure Chemical Vapor Deposition (LPCVD) of 130 nm was deposited as material of the input and output waveguides. The Si_3N_4 layer was processed by a dry etching of 120 nm to define the input and output waveguides. The remaining 10 nm of Si_3N_4 film was used in a next step as a stop etching material. To protect the waveguides, a 1 µm layer of SiO_2 PECVD was deposited. In order to open a top window, both a dry and wet etching processes were performed on the top layer of SiO_2, where the remaining Si_3N_4 layer acts as a stop material. The rest of Si_3N_4 on the windows was removed by phosphoric acid until expositing of the thermal SiO_2. In the top window a dry etching defined the microcantilever shape on the thermal SiO_2 and Si. Next step was to remove all the Si under the microcantilever shape with two consecutive etching steps, a fast and dry etching to remove a 295 µm of Si and a wet etching to remove the remaining 5 µm of silicon under the microcantilever. Finally, to adjust the final 350 nm thickness of OWC devices, a dry etching was performed under the SiO_2 microcantilevers.

In order to increase the optical coupling at the input waveguides and reduce the optical dispersion at the output waveguide, a polish process was applied to the input and output side of each chip (Figure 2-C), this process also help in reducing the coupling efficiency differences between each input waveguide within the same chip. For the polishing process, the chip is fixed to a stage with two PDMS films with an open window to avoid any damage to the microcantilevers. The stage is fixed in a polishing machine and the input and output side of the chip is polishing using a three sand paper of 0.9 µm, 0.6 µm and 0.3 µm, respectively, for 5 minutes each of them; the pressure between the chip and the sand paper is manually adjust until the side is polished.

Due to the complexity of the fabrication process, the OWC devices suffered an over etch during the deep silicon etching process (Figure 2-E-7). This generated a non-square OWC thickness shape, with up to 500 nm of thickness difference between the middle of OWC and the clamp region that can reduce the optical efficiency at the interface and produces differences in the initial deflection of each microcantilever. However, some of the chips might be used for optical characterization and biorecognition evaluations.

2.3 Experimental setup

The experimental set-up is based on a single laser–single acquisition channel in order to evaluate the optical response of each OWC (Figure 3-A and Figure 3-B). The OWC chip, with the microfluidic cell, is placed between the light source and the acquisition photodiode system. The microfluidic cell is mounted on a motorized single axis platform (PI M126.PD1) to select the microcantilever to be evaluated or to perform a sequential detection of the response of several microcantilevers in the array.

The laser beam from a temperature controlled laser diode (Mitsubishi ML101J27), working at 660 nm and power of 120 mW, is coupled into the input waveguides using direct focusing with an objective lens (Leica 40X, NA 0.66). Previous to the objective, an aspheric lens of f = 11 mm, an optical insulator and a $\lambda/2$ film (to control the polarization of the beam) are used to achieve a collimated beam and to avoid back reflections that could produce instabilities in the laser emission. The output laser power after passing all optical components is 30 mW. The laser diode and the optical ensemble are mounted on a piezoelectrically controlled XYZ platform with a resolution of 20 nm and a maximum displacement of 20 μm (Thorlabs MAX312/M), which render in a high precision performance through an automatic coupling algorithm of the light into the input waveguides.

The OWC chip is inserted into a Poly(methyl methacrylate) (PMMA) microfluidic cell with a common fluidic channel for the entire array, made into a 0.5 mm poly(dimethyl siloxane) (PDMS) thin layer in contact with the top and bottom surface of the OWC chip. The sealing was achieved by applying pressure by a couple of screws on each side, allowing reusing the microfluidic cell several times. The microchannel dimensions are 500 µm wide and 200 µm thick. The PMMA microfluidic cell has one inlet port and two outlets, to assure a complete liquid exchange under the microcantilevers (Figure 3-C). The solution is injected from the top with a flow rate of 10µl/min, on one side of the channel, filling the channel and the window inside the optical device, and flowing out through both output ports using a peristaltic pump (Gilson Minipuls 3) which can produce a flow rate from 0.3 µl/min up to 30 µl/min.

In order to minimize undesired fluid effects into the OWC displacement, we previously modelled the flow inside the microfluidic cell once integrated with the microcantilever array (Figure 3-D) using finite-element analysis software (COMSOL multiphysics). From these simulations we obtained the force that the fluid produces to each OWC inside the fluid cell. For the OWC close to the fluid cell output (where the force is minimal), the force is 0.042 N/m^2 with downward sense, for a fluid flow rate of 10 µl/min. This force induces a 5.68 nm displacement of the microcantilever free end, which is almost 60 times lower than for a typical cantilever biosensor displacement[16]. For a surface stress difference of 0.05 N/m, the displacement is around 339.8 nm. This result confirms the low influence in the OWC movement of the fluid streaming and the peristaltic pump pulses.

The light exiting the output waveguide is collected with another objective lens (Leica 40X, NA 0.66), and focused into a silicon photodetector (Thorlabs SM05PD1A). A diaphragm avoids ambient light to affect the collected signal. This optical group is mounted on a manual XYZ platform to easily collect the light into the photodetector.

The acquisition system consists in a commercial current to voltage amplifier (Thorlabs PDA200C) where the output signal is acquired by a commercial acquisition card (National Instruments, PCI–6259). The data acquisition and the platforms movement are synchronized by a custom Labview application. Either selecting a single microcantilever or a sequential monitoring of several devices, the system continuously maximizes the light coupled into each waveguide automatically. This minimize the drifts of the signal due to losses in the light coupling and improves the reproducibility in the input coupling efficiency, providing stability during the temporal evolution of the optical signal. The algorithm is based on the Nelder-Mead method [17] and uses the output optical power to search the best position of the laser beam focus into the waveguide, reaching the maximum coupling efficiency after few seconds. To monitor all the operations, a microscope camera (Dinolyte) is placed on top of the microfluidic cell.

2.4 Sensitivity of the OWC devices

To employ the OWC as a biosensor, a requisite is to achieve a high sensitivity. Therefore, the deflection noise density (DND) need to be considered to obtain the minimal detectable deflection (MDD), defined as the deflections that produces an optical power change at the noise level [18]. There are several sources of noise that affect the system performance, such as the laser noise, the microcantilever vibration due to thermal noise, the acquisition system noise, and the shot noise of the photodetector. To obtain the theoretical MDD_{sh}, the shot noise current, generated by the photodetector as the single source of noise, is first considered. Using the root-mean-square (rms), the MDD_{sh} can be calculated as [19]:

$$DND = \frac{MDD}{\sqrt{\Delta f}} \tag{1}$$

$$MDD_{sh} = \frac{1}{\sqrt{SNR}} = \sqrt{\frac{2e\eta\Delta f}{S^2 P_{in}\gamma}} \tag{2}$$

where $e = 1.6 \times 10^{-19}$ C is the electron charge, γ is the photodetector efficiency, P_{in} is the input power, η is the device efficiency, S is the sensitivity and Δf is the spectral bandwidth, respectively. Using the data obtained from simulations for a Si_2O microcantilever of 350 nm of thickness, 100 μm length and 30 μm wide, with a 1 μm gap and a Si_3N_4 waveguides of 130 nm thickness, and considering a microcantilever bending equal to zero, we obtained an optical sensitivity of $S = 4.88 \times 10^{-2}$ nm^{-1}, and a device efficiency of $\eta = 0.197$. For an input power of $P_{in} = 4.97$ mW and a photodetector efficiency of 0.314 A/W, obtained from the experimental setup, the DND_{sh} due to the shot noise is $0.13\, fm/\sqrt{Hz}$, with a dynamic range of 105.1 nm by a zero OWC displacement. At the maximum sensitivity the DND_{sh} is $0.10\, fm/\sqrt{Hz}$, with a maximum dynamic range of 359.5 nm, but for obtain these values the OWC must be displaced 93.8 nm (Figure 1-D) These results improves the MDD_{sh} obtained by other authors with similar working principle devices [11,19–22]. Besides the shot noise, the dynamic behavior of the microcantilever must be also considered. The Brownian noise due to the thermal noise, DND_{br} is:

$$MDD_{br} = \sqrt{\frac{2k_b T\Delta f}{\pi Q k f_0}} \tag{3}$$

where k_B is the Boltzmann constant, T is the temperature, Δf is the bandwidth, k is the microcantilever spring constant, f_0 is the microcantilever resonance frequency and Q is the nanomechanical quality factor. For a 100x30x0.35 μm Si_2O microcantilever, with $k = 0.023$ N/m, $f_0 = 31.9$ kHz and $Q = 3.31 \times 10^{-4}$, the DND_{br} obtained is 0.22 $pm/\sqrt{Hz}$. Considering the current to voltage amplifier noise of 200 nA for its full-scale, the DND_{iv} is 13.1 $pm/\sqrt{Hz}$. As a result, the DND_{iv} is higher than the DND_{br}, and therefore, we cannot use the dynamic mode. However, it must be noted that this DND_{iv} is lower than the values previously reported for biorecognition processes [23], which validate the suitability of our system for biosensing applications.

3 Results and discussion

3.1 Optical response characterization

In order to determinate the optical response of the OWC deflection, a second silicon microcantilever was used to push the OWC under characterization. This second cantilever was installed over a structure attached to a motorized nano-stage with 20 nm resolution (Thorlabs MAX312/M). We performed forwards and backwards movements of the silicon microcantilever, contacting the OWC at the free end, and bending it during the forward movements. During the backwards movements, the silicon microcantilever maintained the contact with the OWC even after recovering the initial contact position due to electrostatic forces, producing an upward deflection of the OWC and allowing the measurement of the complete optical profile. The vertical movement of the second cantilever is synchronized by software with the acquisition of the optical output for the OWC.

Figure 4-A shows the comparison of the free end displacement between a simulated OWC and a real OWC response. The efficiency difference between them can be explained mainly by the contact between both cantilevers and by the non-ideal lateral sides of the OWC, which increase light dispersion at the interfaces. Other factor contributing to this difference is the no-rectangular OWC shape at the microcantilever clamp and the free end that reduces the efficiency coupling between the input waveguide and the microcantilever.

Because the microcantilever is the core of an optical waveguide with the surrounding medium as cladding layers, changes on the refractive index of this cladding medium can affect the propagating light inside the microcantilever. This effect is minimal when the OWC has out-of-plane single-mode behavior. To evaluate the refractive index influence, several dilutions of ethanol/water, with known refractive index, were injected into the microfluidic cell, previously stabilized in water.

Figure 4-B shows the temporal evolution of the optical power measured during the injection of the different dilutions of ethanol/water. Changes in the refractive index produce a jump of the output efficiency; as the ethanol concentration increases, the refractive index increases, producing a larger jump of the signal. However, refractive index changes of 1% Ethanol ($\Delta n = 5.5x10^{-4}$ RIU) or lower concentrations produce changes in the efficiency lower than 0.05 % over the output signal. This refractive index change is two orders of magnitude larger than the refractive index changes expected during a biorecognition process, and therefore we can assume that this is the mechanism of the OWC deflection that induces the main optical output changes.

3.2 Polyelectrolytes monolayers assembly

We have evaluated the OWC deflection due to the surface stress differences induced by oppositely charged polyelectrolytes layers, formed by electrostatic affinity, with about 6 nm of thickness by each bilayer [24], over one side of the microcantilever. To achieve the selective adsorption of the polyelectrolyte over only one side of the microcantilever, a gold layer of 15 nm was previously deposited on the top of the OWC chip, with a Ti layer of 2 nm to improve the adhesion between the gold and the microcantilevers. The metallic layers cause a loss of some of the transmitted power, but the exiting power is more than enough for performing the experiments. To produce the surface stress difference between the OWC surfaces, the polyelectrolytes layers must be grown only in one side of the OWC. Therefore, we decided to block the gold layer by immobilizing 10 mg/mL of a protein to a SH-PEG-COOH thiol layer previously deposited. The initial position of the OWC is critical to understand the deflection direction along the experiments; we observed from SEM images that the OWC was downward bended (Figure 2-D). Figure 5-A shows the OWC bending scheme for each stage of the experiment. The gold deposition generates an upward deflection, which changes with the thiol layer, producing a downward deflection[25,26].

Once the gold layer was blocked, subsequent solutions of the polycation poly (diallyldimethylammonium chloride) (PDDA, MW = 400k–500k) and polyanion poly(sodium 4-styrenesulfonate) (PSS, MW = 70k) polyelectrolyte monolayers were injected, with a concentration of 2% in water to minimize the layer thickness.

The subsequent injection of PDDA and PSS resulted in the in-flow formation of polyelectrolyte multilayers on the SiO_2 backside of the microcantilever, as show in Figure 5-B. The refractive index of the polyelectrolytes solutions is about 1.50, which resulted in an initial change of the signal due to the refractive index change of the medium, hiding the temporal response of the microcantilever due do the electrostatic formation of the layer over the surface. Once the water reaches the microcantilever and washes it, a net signal change is observed after each polyelectrolyte layer formation, indicating a change in the surface stress generated on the microcantilever, and therefore, a net binding after the layer formation. This demonstrates that even when the refractive index of the medium can alter the signal evolution, it is possible to detect the deposition event occurring on the microcantilever by only comparing the power before and after the binding process. From Figure 5-B it can be observed an increment in the OWC optical response with each polyelectrolyte layer due to the upward bending of the OWC, that increases the alignment with the output waveguide. Also, from Figure 5-B it can be observed an increment in the OWC optical response on the second polyelectrolyte bilayer, this is caused by an increment of thickness of each layer, due to the changes in the roughness of the surface [24].

3.3 Human growth hormone immunoassay

To demonstrate the performance of the OWC as a biosensor, we carried out the detection of the human growth hormone (hGH), an important hormone secreted by the pituitary gland, essential for the normal growth. Both excess and deficiency of this hormone can be related with a problem in the pituitary gland, caused by a pituitary tumor, malformation or damages [27]. To this end, the top side of the microcantilever was blocked with a bobine serum albumin protein (BSA), physically adsorbed in order to obtain a difference in the surface stress between the OWC sides. The BSA, with a concentration of 3 mg/mL in a 10 mM acetate buffer of 4.7 pH, was deposited only over the top side using an in-house microdeposition unit (NanoeNablerTM system from BioForce Nanosciences, USA), performed by the ICTS "NANBIOSIS". Molecules to be printed are loaded into the reservoirs of the surface patterning tool (SPT), based on cantilevers (SPT-S-C30R), by using a 0.5 µl pipette. The SPT was previously cleaned with hot organic solvents and under UV/Ozone cleaner (UV/Ozone ProCleaner TM, BioForce Nanosciences, USA) at least during 40 minutes, to facilitate wettability and fluid flow though the cantilever. Relative humidity was adjusted to 50%, and after the spotting the chip was incubated for 1h at room temperature and 50% ambient humidity, to achieve a uniform physically linked protein layer. The top side of the chip was previously cleaned with oxygen plasma to remove any organic dirty and to increase the negative charges over the surface, enhancing the electrostatic adsorption of the BSA protein (which has a positive charge under the solution conditions employed). Finally the sensor devices were inserted into the microfluidic cell to continue with an in-flow biofunctionalization and the biosensing of the hormone in real time.

Figure 6-A shows the process of the in-flow biofunctionalization of the back side of the microcantilever with the selective monoclonal antibody. To achieve a well-packaged and stable receptor layer we used the self-assembled monolayer (SAM) chemistry based on a silane with a carboxylic acid group at the end

(Carboxyethylsilanetriol Sosium Salt – CTES), and the subsequent covalent binding of the antibody by activation of the carboxylic group. The silanization protocol was previously optimized by our group and ensure the anti-hGH covalent binding to the cantilever surface [28]. In Figure 6-B, the first change corresponds to the formation of a silane monolayer (CTES) over the microcantilever back side. Next, a mix solution of EDC/NHS in MES buffer was injected to activate the carboxylic groups of the silane layer. Right after, the antibody solution (anti-hGH, 18 μg/mL in PBS) was injected, reacting covalently with the receptor layer, and producing a net change in the detected power after the base solution (water) washes the surface and recovers the refractive index before the injection (Figure 6-C).

After the formation of the bioreceptor layer over the optical transducer, we performed the immunoassay experiments, in a PBS 1x buffer. The first injection of 5 μg/mL of hGH in PBS 1x resulted in a bending deflection and output power change (Figure 6-D). During the biointeraction reaction the signal oscillates, maybe due to the removing of proteins non–specifically immobilized. An injection of HCl 10 mM, for regenerating the surface, break the non-covalent bonds between the antibody and the hormone, restoring the initial power value, which demonstrate the regeneration of the surface.

A second injection of the hormone produced a efficiency change in the monitored power of 0.11 %, even higher than the first one (Figure 6-E), with a more stable signal, probably due to a better cleaning of the surface of antibodies not properly bonded during the HCl regeneration cycle. A second injection of HCl 10 mM recovered again the initial output power.

Conclusions

We have optimized the design, fabrication and experimental system assembly of an array of photonic microcantilevers for biosensing applications. The OWCs were fabricated and characterized using a custom software and optical setup, with an auto-alignment system that obtain the maximum output signal, increasing the measurement reproducibility, the signal to noise ratio and, therefore, the Minimum Detectable Deflection (MDD). With this setup we measured the OWC output response as a function of the cantilever free end position, obtaining a theoretical deflection noise density $\mathrm{DND_{sh}}$ of $0.13 fm/\sqrt{Hz}$ due to the shot noise, lower than other MEMS designed until now, and an experimental $\mathrm{DND_{iv}}$ of $13.1\, pm/\sqrt{Hz}$, obtained from the characterization evaluations, that can be even further improve by reduction of the electronic noise.

The influence of the refractive index of the external medium was also evaluated, obtaining a low influence in the output signal for refractive index changes lower than $5.5\text{x}10^{-4}$ RIU. To demonstrate the capabilities of the OWC as a biosensor, we performed the detection of the human growth hormone at 5 μg/mL concentration, including regeneration cycles of HCl 10 mM, demonstrating the excellent capabilities of this optomechanical device as a biosensor.

Acknowledgements

Authors acknowledge the financial support of the Generalitat de Catalunya and has support from the Departament d'Universitats, Recerca i Societat de la Informació de la Generalitat de Catalunya (2014 SGR 624), ICN2 is the recipient of Grant SEV-2013-0295 from the "Severo Ochoa Centers of Excellence" Program of Spanish MINECO.The surface blocking process was performed by the ICTS "NANBIOSIS", more specifically by the microdeposition unit (NanoeNablerTM system from BioForce Nanosciences, USA), unit of the CIBER in Bioengineering, Biomaterials & Nanomedicne (CIBER-BBN)

Biogrqaphies

David Fariña Santana: David Fariña is Ph. D. at the Nanobiosensors and Bioanalytical Applications group at the Ciber BBN and the Catalan Institute of Nanoscience and Nanotechnology (ICN2) of the Spanish National Research Council (CISC), with special interest on software and hardware development for optical biosensors and their integration in a lab-on-chip platforms. He obtained the ME degree and the PhD in Telecommunications Engineering at the University of Las Palmas de Gran Canaria, Spain.

Mar Álvarez: Mar Alvarez is currently a researcher at the Biomedical Applications Group at the Institute of Microelectronics of Barcelona of the Spanish National Research Council (IMB-CNM, CSIC). Her main research interest is focused on the technological development of microfluidics and biosensor devices and its integration on lab-on-a-chip and organ-on-chip platforms for the performance of a wide range of biomedical applications. She obtained her MSc and PhD degrees in Physics from the Autonoma University of Madrid, Spain.

Salomón Marquez: Salomón Marquez received his M.Sc degree in Electrical Engineering from The Center for Research and Advanced Studies of the National Polytechnic Institute (CINVESTAV), Mexico. In 2011 he started a Ph.D. program at the Catalan Institute of Nanoscience and Nanotechnology (ICN2, CSIC) in the Nanobiosensors and Bioanalytical Applications group. Currently he is working on the development of mechanical resonators with embedded microchannels for biosensing applications. His fields of interest include modeling of MEMs, integration of microfluidic applications and development of biomedical sensors.

Carlos Dominguez: Carlos Domínguez received the B.S., M.S., and Ph.D. degrees in chemistry from the Universidad Complutense of Madrid, Spain, in 1980, and 1985, respectively. He became a member of the scientific staff at the Instituto de Microelectrónica de Barcelona (IMB-CNM, CSIC) in 1986. Since 1991 he has been a Senior Scientific Researcher. He is involved in materials and process development for new transducers and sensors. Currently he is working on the development of an integrated optical technology based on silicon for (bio)-chemical sensors and broad-band telecommunications applications.

Laura Lechuga: Prof. Laura M. Lechuga is Full Professor of the Spanish National Research Council (CSIC); Adjunct Professor at the Dept. of Physics&Technology, at the Arctic University (Norway) and Distinguished Visiting professor at the Dept. of Microwaves and Photonics, School of Electrical and Computer Sciences, University of Campinas (Brazil). She is the Head of the Nanobiosensors and Bioanalytical Applications Group in the Catalan Institute for Nanoscience and Nanotechnology (ICN2) in Barcelona (Spain). The principal focus of her research program is the technological development of photonic (plasmonics and silicon-based) and nanomechanical biosensors, their integration in portable lab-on- a-chip platforms and their application in clinical and environmental diagnostics. She is associate editor of the IEEE Photonics Journal, associate editor of the J. Optics and Laser Technology (Elsevier) and is at the Editorial Board of the Journal of Nanobiosensors in Disease Diagnosis and of the Journal of Sensors. She has been nominated as Fellow of the Optical Society (OSA) in 2014. She is a member of Permanent Steering Committees of Advanced Study Course on Optical Chemical Sensors (ASCOS) and Europt(r)ode Conference Series.

References

[1] C.D. Chin, T. Laksanasopin, Y.K. Cheung, D. Steinmiller, V. Linder, H. Parsa, J. Wang, H. Moore, R. Rouse, G. Umviligihozo, E. Karita, L. Mwambarangwe, S.L. Braunstein, J. van de Wijgert, R. Sahabo, J.E. Justman, W. El-Sadr, S.K. Sia, Nat. Med. 17 (2011) 1015–1019.

[2] S.G. Anema, Int. Dairy J. 19 (2009) 198–204.

[3] E.K. Sackmann, E. Berthier, E.W.K. Young, M.A. Shelef, S.A. Wernimont, A. Huttenlocher, D.J. Beebe, Blood 120 (2012) e45–e53.

[4] E. Brouzes, M. Medkova, N. Savenelli, D. Marran, M. Twardowski, J.B. Hutchison, J.M. Rothberg, D.R. Link, N. Perrimon, M.L. Samuels, Proc. Natl. Acad. Sci. 106 (2009) 14195–14200.

[5] L. Wang, R. Yan, Z. Huo, L. Wang, J. Zeng, J. Bao, X. Wang, Q. Peng, Y. Li, Angew. Chem. Int. Ed. 44 (2005) 6054–6057.

[6] C.E. Sims, N.L. Allbritton, Lab. Chip 7 (2007) 423–440.

[7] J. Fritz, M.K. Baller, H.P. Lang, H. Rothuizen, P. Vettiger, E. Meyer, H.-J. Güntherodt, C. Gerber, J.K. Gimzewski, Science 288 (2000) 316–318.

[8] A. Gupta, D. Akin, R. Bashir, Appl. Phys. Lett. 84 (2004) 1976–1978.

[9] T.P. Burg, M. Godin, S.M. Knudsen, W. Shen, G. Carlson, J.S. Foster, K. Babcock, S.R. Manalis, Nature 446 (2007) 1066–1069.

[10] K. Zinoviev, J.A. Plaza, V. Cadarso, L.M. Lechuga, C. Dominguez, in:, Proc. SPIE, 2006, pp. 618607–618607–14.

[11] J.W. Noh, R.R. Anderson, S. Kim, W. Hu, G.P. Nordin, Opt. Express 17 (2009) 20012–20020.

[12] K. Misiakos, I. Raptis, A. Gerardino, H. Contopanagos, M. Kitsara, Lab. Chip 9 (2009) 1261–1266.

[13] M.W. Pruessner, T.H. Stievater, M.S. Ferraro, W.S. Rabinovich, J.L. Stepnowski, R.A. McGill, Lab. Chip 10 (2010) 762–768.

[14] S.J. Ness, R.R. Anderson, W. Hu, D.C. Richards, J. Oxborrow, T. Gustafson, B. Tsai, S. Kim, B. Mazzeo, A. Woolley, G.P. Nordin, IEEE Sens. J. 13 (2013) 959–968.

[15] D. Fariña, M. Álvarez, S. Márquez, C. Dominguez, L.M. Lechuga, J. Phys. Appl. Phys. 48 (2015) 335401.

[16] Y. Arntz, J.D. Seelig, H.P. Lang, J. Zhang, P. Hunziker, J.P. Ramseyer, E. Meyer, M. Hegner, C. Gerber, Nanotechnology 14 (2003) 86.

[17] J.A. Nelder, R. Mead, Comput. J. 7 (1965) 308 –313.

[18] G.G. Yaralioglu, A. Atalar, S.R. Manalis, C.F. Quate, J. Appl. Phys. 83 (1998) 7405.

[19] K. Zinoviev, C. Dominguez, J.A. Plaza, V.J.C. Busto, L.M. Lechuga, J. Light. Technol. 24 (2006) 2132–2138.

[20] G. Putrino, A. Keating, M. Martyniuk, L. Faraone, J. Dell, J. Light. Technol. 30 (2012) 1863–1868.

[21] C. Schönenberger, S.F. Alvarado, Rev. Sci. Instrum. 60 (1989) 3131–3134.

[22] G. Putrino, M. Martyniuk, A. Keating, L. Faraone, J. Dell, Nanoscale 7 (2015) 1927–1933.

[23] R. McKendry, J. Zhang, Y. Arntz, T. Strunz, M. Hegner, H.P. Lang, M.K. Baller, U. Certa, E. Meyer, H.-J. Güntherodt, C. Gerber, Proc. Natl. Acad. Sci. 99 (2002) 9783–9788.

[24] R.A. McAloney, M. Sinyor, V. Dudnik, M.C. Goh, Langmuir 17 (2001) 6655–6663.

[25] M. Godin, V. Tabard-Cossa, Y. Miyahara, T. Monga, P.J. Williams, L.Y. Beaulieu, R. Bruce Lennox, P. Grutter, Nanotechnology 21 (2010) 075501.

[26] J. Mertens, M. Calleja, D. Ramos, A. Tarýn, J. Tamayo, J. Appl. Phys. 101 (2007) 034904.

[27] J. Treviño, A. Calle, J.M. Rodríguez-Frade, M. Mellado, L.M. Lechuga, Talanta 78 (2009) 1011–1016.

[28] A.B. González-Guerrero, M. Alvarez, A.G. Castaño, C. Domínguez, L.M. Lechuga, J. Colloid Interface Sci. 393 (2013) 402–410.

Figure Caption

Figure 1. Optical Waveguide Cantilever working principle: a) OWC 3D view and vertical cross section b) Microcantilever bending due to surface stress c) OWC optical efficiency response and theoretical sensitivity as a function of its free end displacement for 100 μm length, 250 nm of thick and 1 μm of gap microcantilever d) Relation between the OWC efficiency, sensitivity and deflection noise density (DND) due to the shot noise as a function of the OWC displacement on the deflection range.

Figure 2. Fabricated out-of-plane single-mode OWC: a) OWC chip dimension, b) Detail of an OWC array, c) Polished Input waveguide, d) Detail of an out-of-plane single mode OWC, e) Summary of the complete fabrication process (*SEM Images artificially colored*).

Figure 3. Optical waveguide cantilever setup: a) Scheme of the optical setup, b) Experimental optical setup with fluidic cell, c) Cross section of the microfluidic cell d) Fluid velocity simulation in the fluid cell cross section. The color intensity represents the magnitude and the color is related with the direction of the fluid (red – up, blue - down).

Figure 4. Characterization of the Optical Waveguide Cantilever, a) Comparison of the response between simulated and evaluated OWC using a second microcantilever b) Refractive index changes for solutions 10%, 5% and 1% of ethanol/water.

Figure 5. A) Deflection state of the OWC in each stage of the poly-electrolyte deposition experiment. B) OWC response to successive creation of polyelectrolyte PDDA/PSS bilayers.

Figure 6. Biosensor immunoassay of the Human growth hormone: a) Schematic of the complete immunosensingr experiment for the detection of hGH b) CTES Silane monolayer formation, c) Activation of the carboxylic groups of the silane layer with EDC/NHS and immobilization of the anti-hGH monoclonal antibody, d) hGH biodetection and regeneration process, e) Second hGH detection after the regeneration step and subsequent regeneration surface process.

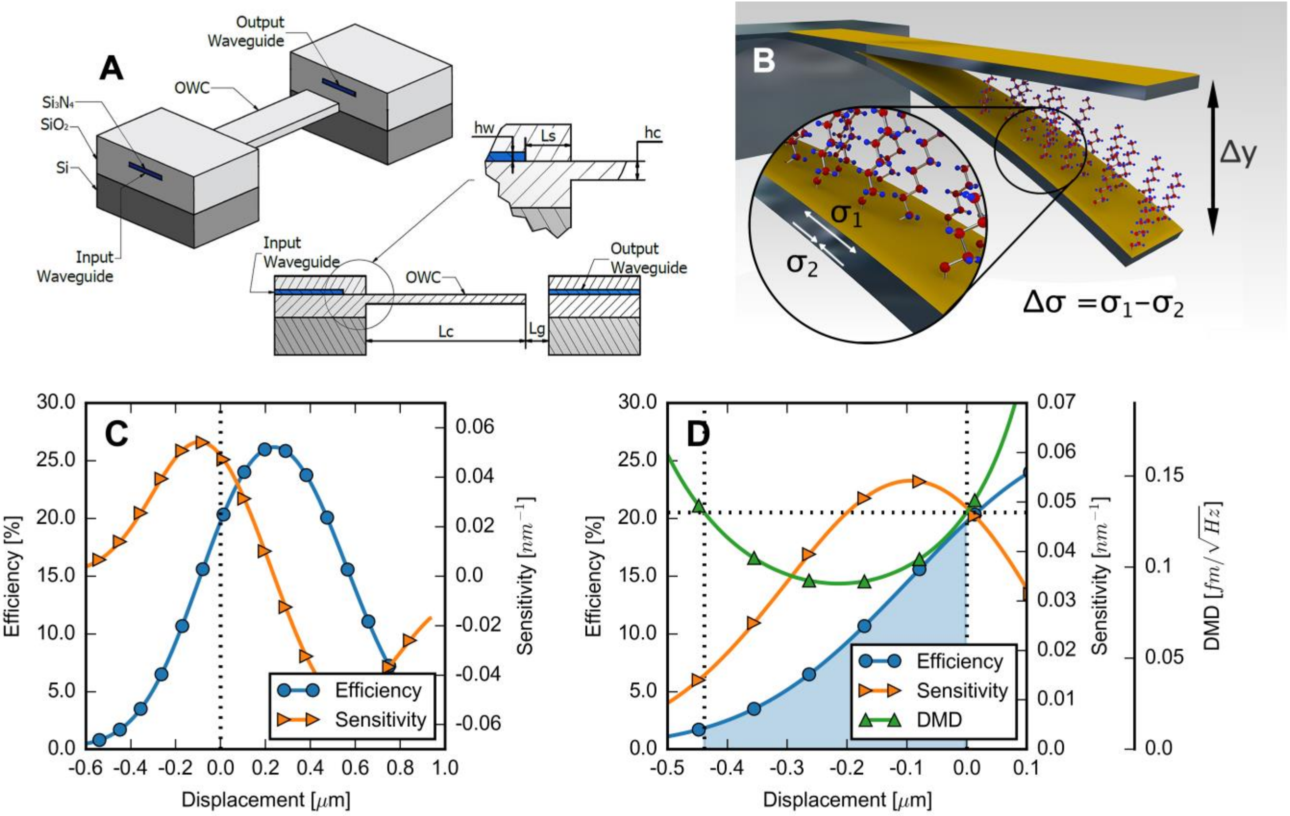
A
Output Waveguide
OWC
Si3N4
SiO2
Si
Input Waveguide
hw
Ls
hc
Input Waveguide
OWC
Output Waveguide
Lc
Lg
B
Δy
σ1
σ2
Δσ =σ1−σ2
C
Efficiency [%]
Sensitivity [nm−1]
Displacement [μm]
30.0
25.0
20.0
15.0
10.0
5.0
0.0
0.06
0.04
0.02
0.0
-0.02
-0.04
-0.06
-0.6
-0.4
-0.2
0.0
0.2
0.4
0.6
0.8
1.0
Efficiency
Sensitivity
D
Efficiency [%]
Sensitivity [nm−1]
DMD [fm/√Hz]
Displacement [μm]
30.0
25.0
20.0
15.0
10.0
5.0
0.0
0.07
0.06
0.05
0.04
0.03
0.02
0.01
0.0
0.15
0.1
0.05
0.0
-0.5
-0.4
-0.3
-0.2
-0.1
0.0
0.1
Efficiency
Sensitivity
DMD

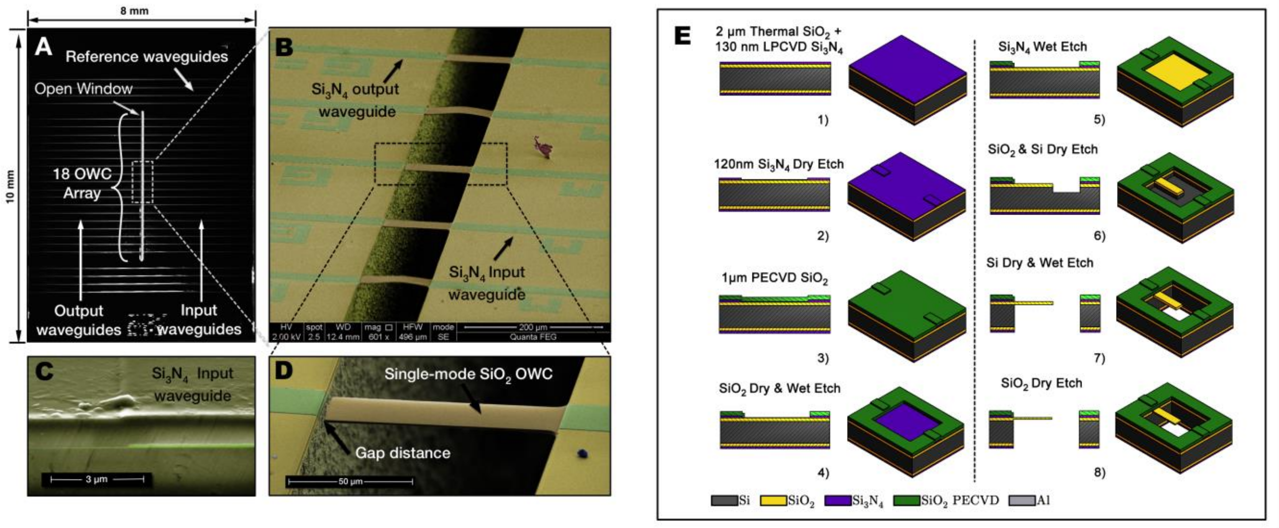
8 mm
10 mm
A
Reference waveguides
Open Window
18 OWC Array
Output waveguides
Input waveguides
B
Si_3N_4 output waveguide
Si_3N_4 Input waveguide
HV 2.00 kV spot 2.5 WD 12.4 mm mag 601 x HFW 496 µm mode SE
200 µm
Quanta FEG
C
Si_3N_4 Input waveguide
3 µm
D
Single-mode SiO_2 OWC
Gap distance
50 µm
E
2 µm Thermal SiO_2 + 130 nm LPCVD Si_3N_4
1)
120nm Si_3N_4 Dry Etch
2)
1µm PECVD SiO_2
3)
SiO_2 Dry & Wet Etch
4)
Si_3N_4 Wet Etch
5)
SiO_2 & Si Dry Etch
6)
Si Dry & Wet Etch
7)
SiO_2 Dry Etch
8)
Si
SiO_2
Si_3N_4
SiO_2 PECVD
Al

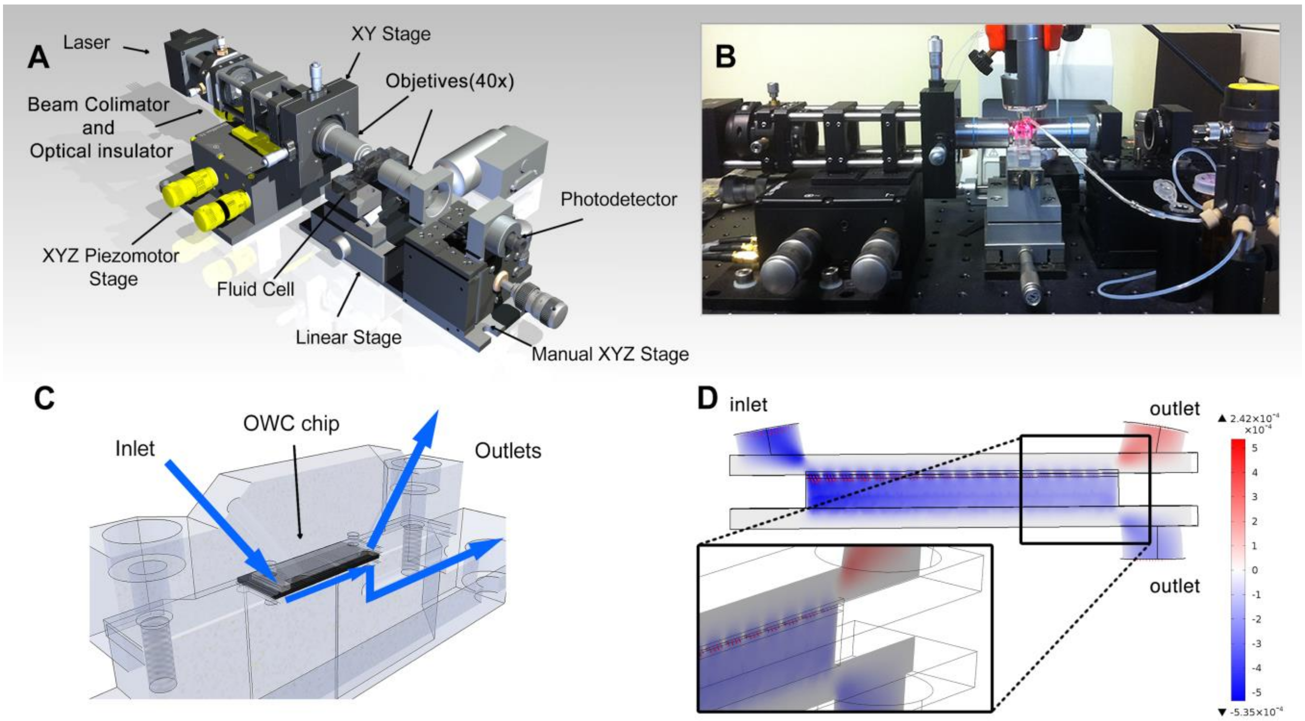
A
Laser
Beam Colimator
and
Optical insulator
XY Stage
Objetives(40x)
Photodetector
XYZ Piezomotor
Stage
Fluid Cell
Linear Stage
Manual XYZ Stage
B
C
Inlet
OWC chip
Outlets
D
inlet
outlet
outlet
▲ 2.42×10⁻⁴
×10⁻⁴
5
4
3
2
1
0
-1
-2
-3
-4
-5
▼ -5.35×10⁻⁴

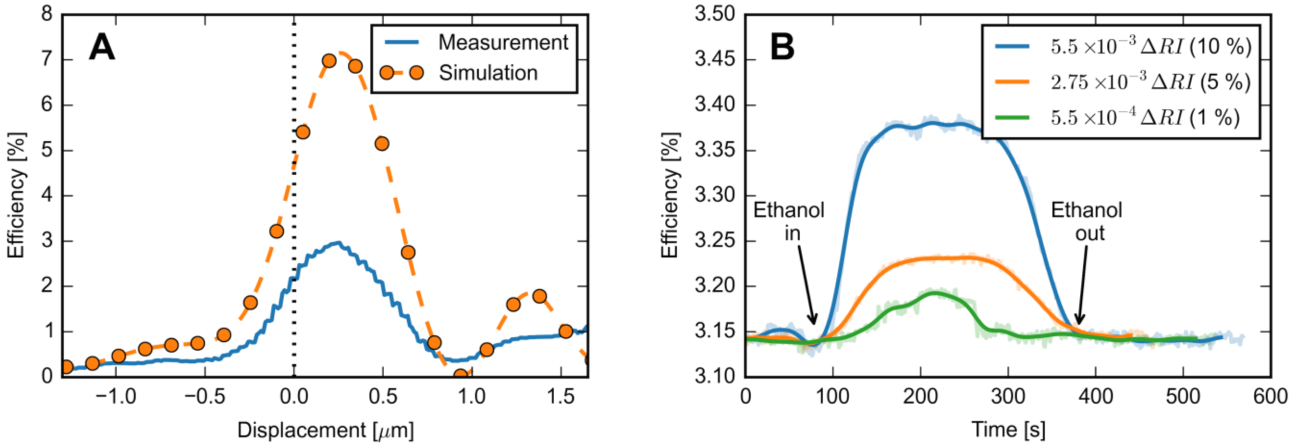
A
Measurement
Simulation
Efficiency [%]
Displacement [μm]
0
1
2
3
4
5
6
7
8
−1.0
−0.5
0.0
0.5
1.0
1.5
B
$5.5 \times 10^{-3}\,\Delta RI$ (10 %)
$2.75 \times 10^{-3}\,\Delta RI$ (5 %)
$5.5 \times 10^{-4}\,\Delta RI$ (1 %)
Ethanol in
Ethanol out
Efficiency [%]
Time [s]
3.10
3.15
3.20
3.25
3.30
3.35
3.40
3.45
3.50
0
100
200
300
400
500
600

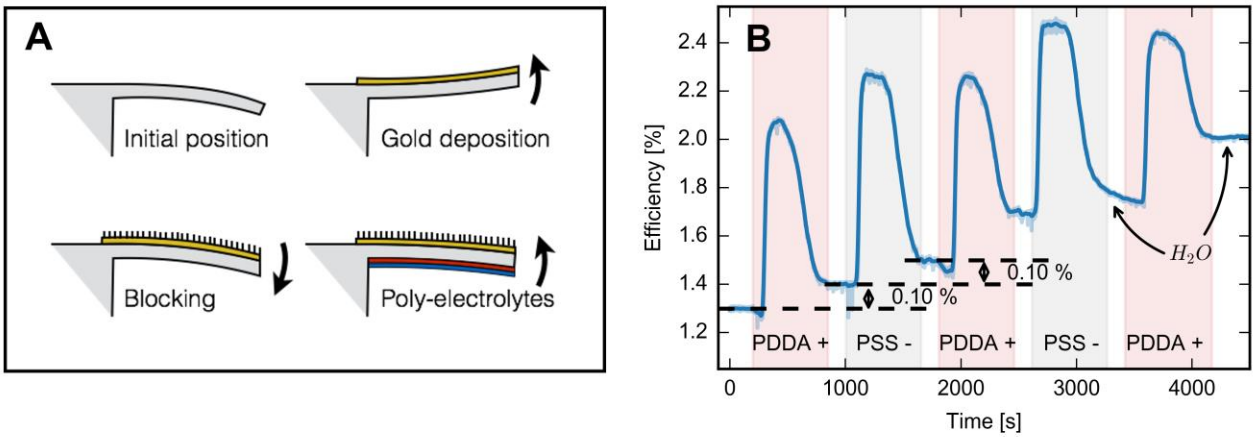
A
Initial position
Gold deposition
Blocking
Poly-electrolytes
B
Efficiency [%]
2.4
2.2
2.0
1.8
1.6
1.4
1.2
0.10 %
0.10 %
H_2O
PDDA +
PSS -
PDDA +
PSS -
PDDA +
0
1000
2000
3000
4000
Time [s]

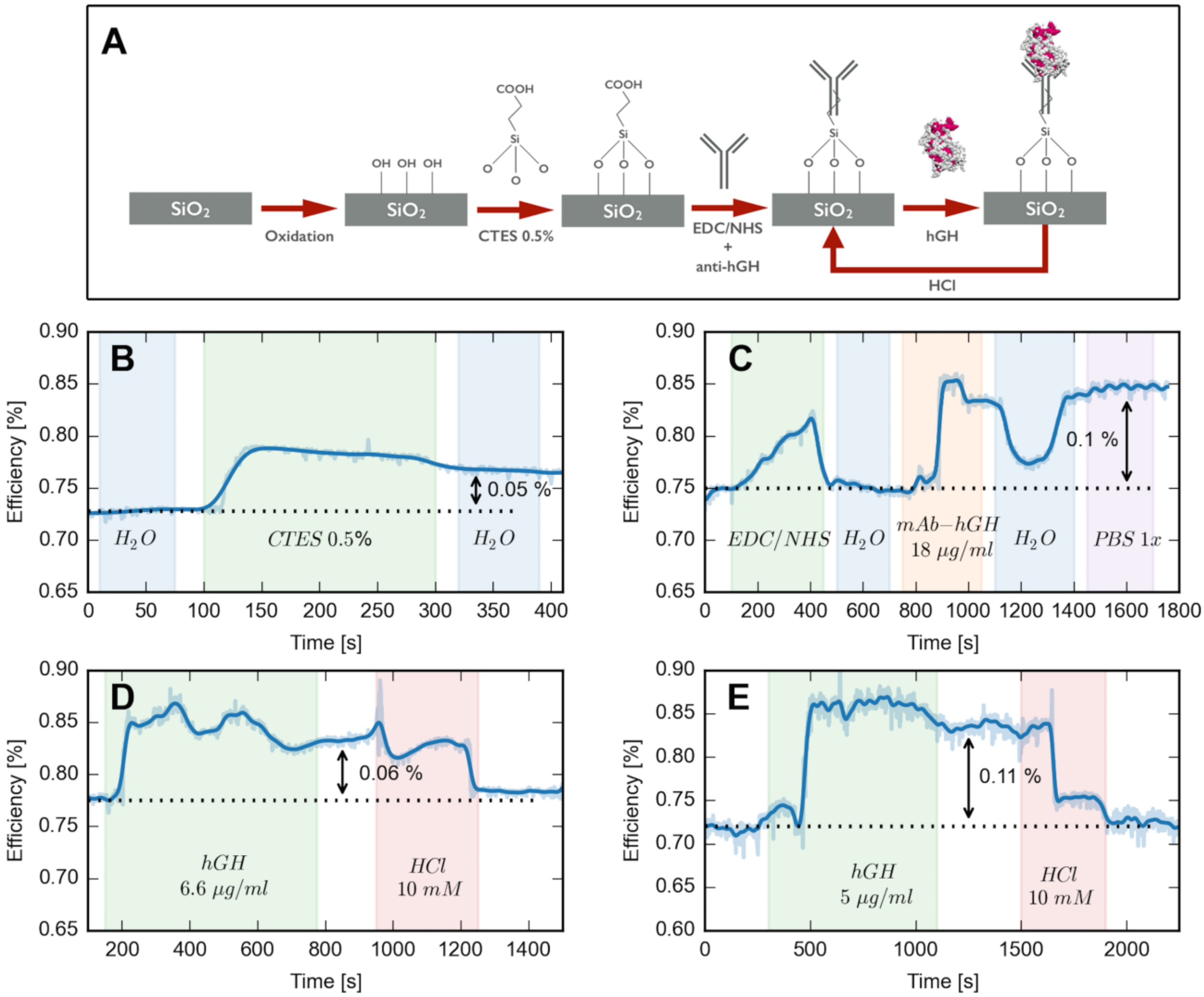
A
SiO2
Oxidation
OH OH OH
CTES 0.5%
COOH
Si
EDC/NHS
+
anti-hGH
hGH
HCl
B
Efficiency [%]
Time [s]
H2O
CTES 0.5%
0.05 %
C
EDC/NHS
mAb−hGH 18 μg/ml
PBS 1x
0.1 %
D
hGH 6.6 μg/ml
HCl 10 mM
0.06 %
E
hGH 5 μg/ml
0.11 %
0.90
0.85
0.80
0.75
0.70
0.65
0.60